IOP Publishing Journal of Optics
J. Opt. 20 (2018) 105502 (10pp) https://doi.org/10.1088/2040-8986/aadef7

Investigating the non-radially polarized component of terahertz wave emission during single-colour femtosecond laser filamentation in air

Jiayu Zhao[1], Hui Gao[2], Shichang Li[1], Chang Liu[1], Yamin Chen[1], Yan Peng[1,3] and Yiming Zhu[1,3]

[1] Shanghai Key Laboratory of Modern Optical System, Terahertz Technology Innovation Research Institute, University of Shanghai for Science and Technology, Shanghai 200093, People's Republic of China
[2] School of Science, Tianjin Polytechnic University, Tianjin 300387, People's Republic of China

E-mail: gaohuioptics@163.com, py@usst.edu.cn and ymzhu@usst.edu.cn

Received 28 April 2018, revised 4 September 2018
Accepted for publication 5 September 2018
Published 17 September 2018

Abstract

Recently, simultaneous emission of radially and non-radially polarized terahertz (THz) pulses during single-colour femtosecond laser filamentation has been reported. In this work, the latter radiation has been specifically investigated, instead of the well-studied THz radial polarization. Briefly, cut-back measurements have verified that the ellipticity of the generated THz pulse with non-radial polarization decreased (became more linearly polarized) with the increasing filament length. The underlying mechanism responsible for this phenomenon is the existence of a propagation effect of THz wave along the filament plasma channel. In this case, the resulted off-axis propagation of THz wave inside the plasma column played a dominant role on the generated non-radial THz polarization, rather than the expected on-axis THz birefringence induced by the high laser intensity. This discovery will greatly renew the understanding of THz emission from plasma sources.

Keywords: terahertz wave, non-radial polarization, filamentation, single colour

(Some figures may appear in colour only in the online journal)

1. Introduction

Terahertz (THz) science and technology has enjoyed an explosive expansion in the past few decades [1–3], attracting intense attention from all over the world. Among multitudinous hot research topics, the development of practical THz sources is absolutely one that has to be mentioned [4, 5]. Femtosecond laser filamentation in air, a unique nonlinear optical phenomenon able to generate a long plasma channel, is one of the most competitive THz sources for its capability of remotely emitting THz wave with broad bandwidth and high intensity [6, 7]. By simply manipulating the position of a filament, THz pulses can be emitted at a remotely located target, minimizing the strong THz energy absorption by water vapour in the atmosphere [8]. In view of various schemes of THz wave generation related to filamentation, single-colour femtosecond laser pumping might be the most convenient method since it can be achieved by simply focusing a commercial Ti:sapphire laser beam in air. Thus, significant efforts have been made to unfold the nature in this field for more than 20 years [7, 9–23]. Several milestones are as follows.

1.1. Radial emission of THz wave with linear/circular polarization

Since the first direct observation of THz wave during single-colour filamentation in 1993 [9], side-emission property of THz wave generation due to longitudinal plasma oscillations

[3] Authors to whom any correspondence should be addressed.

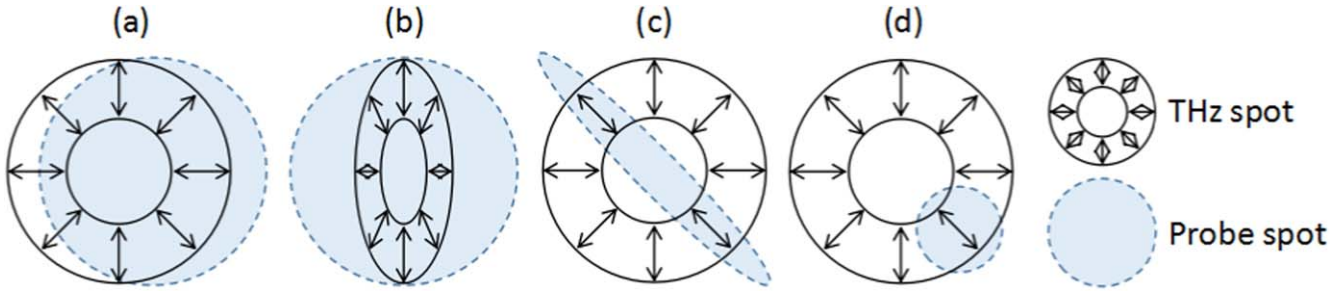

Figure 1. Four possible cases of the interaction between THz and probe spots on the surface of the EO crystal without ideal superposition.

induced by radiative pressure once became a mainstream theory [10]. Back then, one of the significant contributions to the community is from Mysyrowicz's group in France [11–13]. They have experimentally studied the THz radiation in the radial direction of the single-colour filament, and the THz wave has been found to be coherent with linear or circular polarization.

1.2. Conical emission of THz wave with radial polarization

Later in 2007, Mysyrowicz's group for the first time discovered the conical forward THz emission with radial polarization [7], besides the aforementioned side emission [11–13]. By measuring THz polarization and intensity at different points across the THz beam section, the obtained THz beam is found to be radially polarized and has a donut beam shape [7]. This finally turns into the modern view of THz wave generation from a single-colour filament, whose mechanism is generally understood as the consequence of transition Cherenkov emission from the plasma space charge moving behind the ionization front at light velocity [7]. Similar conclusions drawn by experiment or simulation can also be found in the literature, such as [19, 20].

However, controversies arose soon after. Non-radial THz polarization has been frequently reported [15, 21–24]. Different points of view have been brought forward to explain the mechanism of the THz pulse generation by single-colour laser field.

1.3. Forward emission of THz wave with linear polarization

For example, in the work of Bai *et al* [24], THz polarization has been measured to be nearly linear during single-colour filamentation, which cannot be originated from transition-Cherenkov-type radiation [7]. The authors have attributed this linear THz polarization to the transient photocurrent driven by the propagating intense few-cycle laser fields in the plasma [25, 26].

1.4. On-axis emission of THz wave with elliptical polarization

Moreover, Zhang *et al* [21] and Jahangiri *et al* [22] have revealed that the THz beam emission during single-colour filamentation in the air underwent on-axis propagation with elliptical polarization. They suggested that the mechanism of the THz pulse generation could be interpreted by the four-wave mixing (4WM) and parametric decay, respectively.

Nevertheless, in the above self-consistent publications [21, 22, 24], the authors adopted optical elements, such as off-axis parabolic mirrors (OPMs), to collimate and focus the THz beam onto the detectors (electro-optical crystal or bolometer) while measuring the THz radiation polarization, rather than directly solving this issue in different spatial locations after the filament [7]. In this case, any displacement of the probe beam from the central symmetrical position of the focused THz spot on the surface of the EO crystal will probably result in a non-radial THz polarization detection (see figure 1(a)). Even worse, any misalignment of the OPMs may somehow distort the generated THz polarization (see figure 1(b)). Both cases made the observed non-radial THz polarization [21, 22, 24] less convincing.

Finally, the controversial non-radial THz polarization emitted from a single-colour filament has been deeply investigated by Chen *et al* [23] by means of rotating the polarization angle (ϕ) of the pump laser, which is equivalent to rotating the polarization azimuth of the generated THz pulse. If the THz radiation is only in radial polarization during single-colour filamentation, the central symmetry of its polarization 'donut' will not be affected by ϕ. Then, the possible mismatch of THz and probe spots on the EO crystal's surface (figure 1(a)), or the THz polarization distortion resulted from the OPMs' misalignment (figure 1(b)), will always remain the same while ϕ is varied, since all the optical elements are fixed in the meantime, and the final polarization detection result is expected to be independent on ϕ.

However, Chen *et al* [23] have observed that the azimuth of the major axis of the THz ellipse rotated in the same direction by the same angle with the variation of ϕ, which could indicate the existence of non-radially polarized component of THz emission during single-colour filamentation. Afterwards, Chen *et al* [15] have discovered the evolution of THz wave from elliptical into linear polarization by applying an increasing DC external electric field sandwiching the single-colour filament. This has further confirmed the presence of non-radially polarized THz emission.

1.5. THz emission with both radial and non-radial polarization

Recently, Jahangiri *et al* [18] have observed both radially and non-radially (elliptically) polarized THz waves emission from

one single-colour filament simultaneously, but separated in space (conical versus forward). Furthermore, previously, our group has focused these two kinds of THz waves in the forward far field of a single-colour filament in order to make longitudinal and transverse THz waves, between which the phase difference was measured to be $\pi/2$ [27]. This value agrees with the conclusion drawn in [28], where the universal phase relation between longitudinal and transverse fields observed in focused THz beams is $\pi/2$.

1.6. Brief introduction of the current work

In this work, we focused specifically on the non-radially polarized THz radiation during single-colour filamentation, instead of the well-investigated radial polarized one [7, 19, 20]. Efforts have been made to reproduce the elliptical THz polarization result achieved by Chen *et al* [23] with the change of the focal length of the focusing lens from 50 to 100 cm, which lengthened the created filament. The azimuth of the THz ellipse has been experimentally re-confirmed as around 40° [23] induced by a horizontally polarized pump laser. However, a very different ellipticity (almost linearly polarized) was observed, putting forward new challenges to the understanding of THz wave generation from a single-colour filament. Hence, this work is mainly aimed at studying the origin of this unusual THz linear polarization creation.

Briefly, by performing the cut-back (CB) method [29], the recorded THz transient with linear polarization has been found to evolve from elliptical polarization along the plasma filament. On the other hand, numerical simulations based on nonlinear wave equation [29, 30] and one-dimensional negative dielectric (1DND) waveguide model [31, 32] have demonstrated the off-axis propagation of THz wave inside the plasma column. Finally, the generated THz linear polarization has been attributed to the combined effects of either the 4WM [21, 23], or the longitudinal plasma oscillations induced by radiative pressure [10], with the weak local THz birefringence during off-axis propagation. Moreover, the far-field ring-shaped distribution of THz power observed in this work and its frequency dependence could also be interpreted by the THz wave propagation effect.

2. Experimental results and analyses

In this work, we have adopted almost the same experimental configuration and parameters as described in [23]. In brief, a 1 kHz (repetition frequency), 800 nm (central wavelength), 50 fs (FWHM of the temporal width) Ti:sapphire laser pulse with 1 mJ/pulse was focused by a $f = 100$ cm lens, creating a centimeter-scale long single-colour filament in the air as the source of THz radiation. The detection setup was a two-dimensional (2D) THz electro-optical sampling (EOS) system [33, 34], which allowed the achievement of both orthogonal components of a THz electric field.

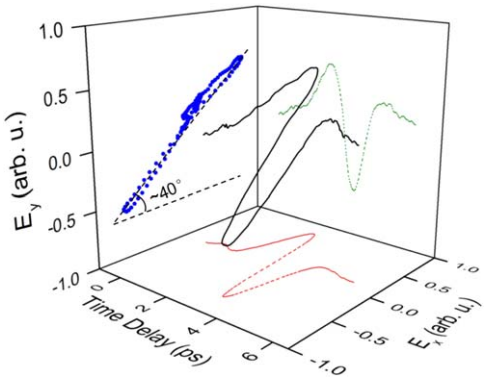

Figure 2. Temporal evolution of the electric field vector of the detected THz pulse with linear polarization.

2.1. Linearly polarized THz pulse emitted from a single-colour filament

In the experiment, a ⟨110⟩ oriented EO crystal (ZnTe) was used to detect the non-radially polarized THz wave emitted from the single-colour filament [21, 23, 27]. The recorded THz electric field waveform is displayed in figure 2. It can be seen that the azimuth of the major axis of the detected THz ellipse was about 40°, similar with that in figure 3 of [23]. However, here the ellipticity ($e = E_{\mathrm{THz,minor\ axis}}/E_{\mathrm{THz,major\ axis}}$) of the THz ellipse was only 0.04, which is in serious disagreement with the previously reported THz elliptical polarization [18, 21–23] whose e is much larger, e.g. around 0.3 according to [23]. Thus, in the following text, we mainly focused on the investigation of this novel THz linear polarization generation.

As for the underlying mechanism of this linear THz polarization emission, it has been reported that THz wave could be generated by femtosecond laser pulses in air through the 4WM process [6, 35]: $\omega_{\mathrm{THz}} = \omega_1 + \omega_2 - \omega_3$, where the angular frequencies ω_1, ω_2 and ω_3 should satisfy $\omega_1 + \omega_2 \approx \omega_3$. Thus, the pump laser spectrum need to be octave-spanned [6]. This condition can be easily fulfilled because in the course of filamentation, the laser spectrum could cover an extremely broad range, extending from ultraviolet to infrared [36–38]. Hence, THz wave with polarization parallel to the horizontally polarized pump laser (referred to as the x direction throughout this paper) can be obtained in air via

$$E_{\mathrm{THz},x} \propto \chi^{(3)}_{xxxx} E_{\omega_3} E^*_{\omega_1} E^*_{\omega_2} e^{i\Delta kL}, \tag{1}$$

where $\Delta k = k_1 + k_2 - k_3$ describes the phase matching condition and L is the effective interaction length. On the other hand, the generation of orthogonally polarized THz wave could be realized mathematically through

$$E_{\mathrm{THz},y} \propto \chi^{(3)}_{yxxx} E_{\omega_3} E^*_{\omega_1} E^*_{\omega_2} e^{i\Delta kL}. \tag{2}$$

Note that $\chi^{(3)}_{yxxx}$ is 0 for an isotopic material like air. However, Xie *et al* [35] have observed nonvanished $\chi^{(3)}_{yxxx}$ when plasma is produced in air by using femtosecond laser pulses, due to the spatial asymmetry of laser induced plasma. Accordingly, in-phase THz pulses could be generated along both orthogonal axes via 4WM process, making a linear THz polarization state

as shown in figure 2, instead of a radially [7] or circularly [22] polarized THz wave. Therefore, the 4WM process has been adopted as the origin of non-radially (linearly) polarized THz wave emission during single-colour filamentation in this work. Nevertheless, this preliminary conclusion still needs further confirmation, since no systematical investigation on the existence and origin of $\chi^{(3)}_{yxxx}$ tensor element within the region of laser-induced air plasma has been reported.

Moreover, it is worth mentioning that, when EOS is performed, one of our experimental routines is to fully cover the THz spot on the EO crystal (ZnTe) with the probe beam. This is achieved by loosely focusing the probe beam to illuminate on the most part of the ZnTe crystal, and then fine adjusting the location of the THz spot on the crystal until the detected THz amplitude remains unchanged. In this case, the recorded THz linear polarization cannot be the result, which is cut out from a radially polarized THz spot by a distorted (or misplaced) probe beam (see figures 1(c) and (d)).

2.2. The variation of THz pulse ellipticity during single-colour filamentation

In order to understand this unusual THz polarization output, its evolution during filamentation might be a valuable clue. Hence next, the CB method [24, 29] has been carried out along the filament to investigate the variation of the orthogonal polarized THz pulses. Note that the concept of 'CB' is borrowed from fibre optics, which originally is to cut a fibre (from one end) into different lengths. In our case, the so-called 'CB' is to block the femtosecond laser filament with a Teflon plate longitudinally moveable in the direction of the laser propagation [29]. It is noteworthy that the CB technique might suffer from side effects, such as the intensity-dependent nonlinear refractive index of the Teflon plate caused by its interaction with the intense laser, or the change of the distance between the ZnTe crystal and the THz focus when the Teflon plate was moved. However, these issues have been discussed in detail in our previous report and have been proved to play negligible roles on the final experimental results [29].

The inserting position of the Teflon plate inside the single-colour filament is defined as z, and $z = 0/2$ cm corresponds to the starting/ending position of the CB measurements. When z varies, different lengths of filaments could be obtained. Meanwhile, 2D-EOS measurements have been performed together with the CB method to detect the emitted THz waveforms in both orthogonal directions, which are shown in figures 3(a) and (b), respectively.

Based on the orthogonal waveforms displayed in figure 3, the retrieved evolution of THz polarization (ellipticity e) is shown in figure 4 as bars. It can be seen that, generally, e decreased with the increasing filament length z, and the final THz output was in linear polarization with e of 0.042 (the last bar in figure 4). For better visualization, three representative THz polarization ellipses have been shown in figure 4 as insets (a)–(c). From figures 4(a)–(c), one can see that the THz amplitude gradually increased with the increasing filament length as expected, while e decreased from 0.185 to 0.101 and

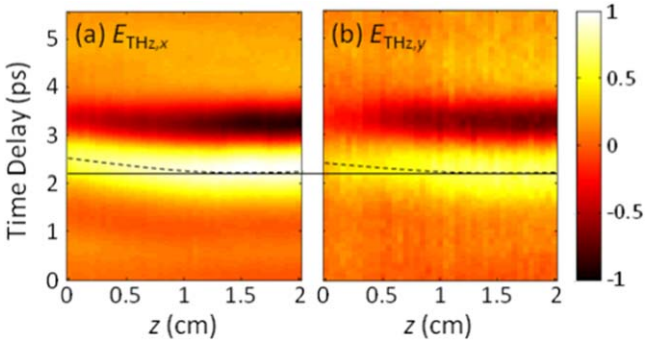

Figure 3. The recorded orthogonal THz waveforms as a function of z. The dashed black lines highlight the temporal advance of the waveform maximum. The horizontal solid line is for contrast.

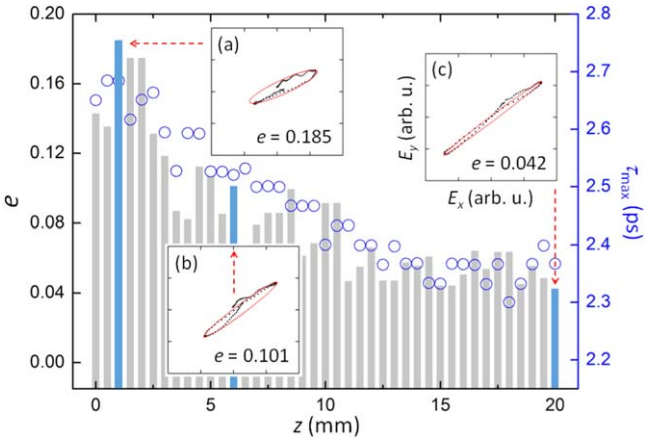

Figure 4. Bars: ellipticity [e] of THz polarization as a function of z. Insets: three representative THz polarization ellipses with e of (a) 0.185, (b) 0.101 and (c) 0.042, respectively. Blue open circles: τ_{max}, which is the temporal displacement of $E_{THz,x}$ maximum.

then 0.042. This novel experimental phenomenon has revealed that the THz polarization spontaneously evolved from elliptical to linear during single-colour filamentation.

Note that at the beginning of the filament, the THz electric field was in elliptical polarization (figure 4(a)), in accordance with the results in [21–23]. Besides, the azimuth of the major axis of the detected THz ellipse was about 40°, also similar with figure 3 in [23]. Therefore, this work might share the same physical origin of non-radially polarized THz wave generation from a single-colour filament with [23], in which the well-known 4WM has been suggested as the underlying mechanism. According to [23], as well as equations (1)–(2) in this work, the process of 4WM creates in-phase orthogonal THz components in directions of x and y, i.e. $E_{THz,x}$ and $E_{THz,y}$, which make a linearly polarized THz pulse. After propagation along the filament, $E_{THz,x}$ and $E_{THz,y}$, ending with different phase delay due to THz birefringence inside the filament, will finally form an elliptically polarized THz pulse.

The above 4WM theory may not satisfy the modern views on THz wave generation from a single-colour filament,

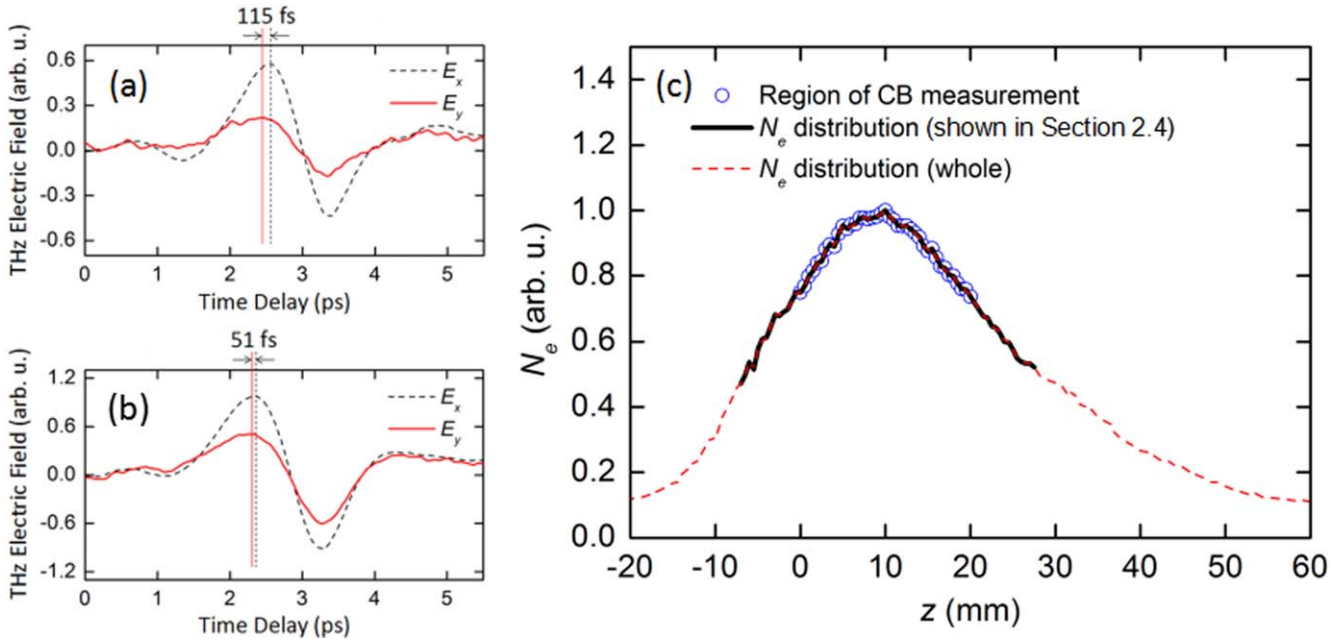

Figure 5. Orthogonal THz electric field waveforms of $E_{\mathrm{THz},x}$ and $E_{\mathrm{THz},y}$ extracted from figure 3 at $z = 1$ mm (a) and $z = 20$ mm (b). The temporal distance between the maximums of $E_{\mathrm{THz},x}$ and $E_{\mathrm{THz},y}$ is about 115 fs (a) or 51 fs (b). (c) N_e distributions, for the cut-back (CB) measurement (blue open circles from $z = 0$ to $z = 20$ mm); shown in section 2.4 (solid black line from $z = -5$ to $z = 25$ mm); as the original data (dashed red line from $z = -20$ to $z = 60$ mm).

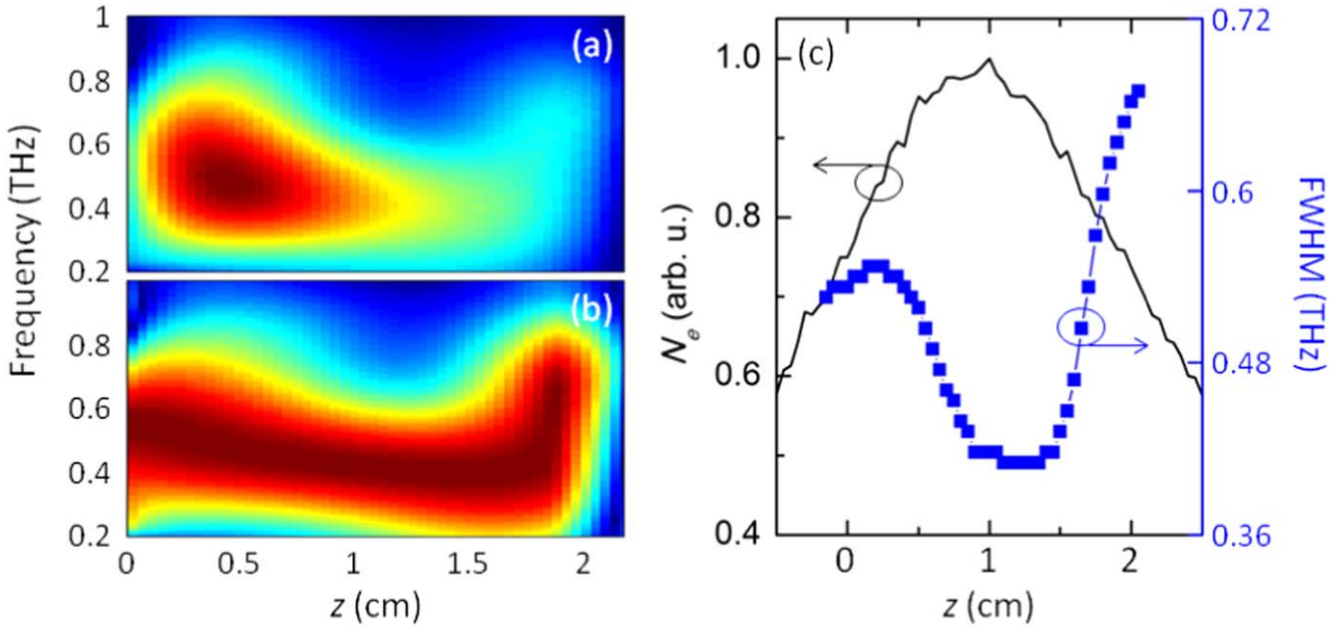

Figure 6. (a) THz spectra emitted from each z point. (b) The normalized results of (a). (c) Distribution of N_e (black line) versus THz spectral FWHM (blue squares) as a function of z.

since it was developed for preliminary and rough description of the THz emission process in 2008. Another possible mechanism responsible for our detection of the non-radially polarized THz wave is the side emission of THz wave with linear polarization, theoretically predicted by [10] and experimentally verified by [12]. Recently, it has been suggested that the radial emission of THz wave can also be guided along the filament to make a forward THz emission mode [39]. Probably, that is what has been detected in this work.

Overall, in the experiment, non-radially polarized THz wave was created, either by 4WM process [23] or by longitudinal plasma oscillations [10], both of which radiate THz wave in linear polarization. After propagation along the

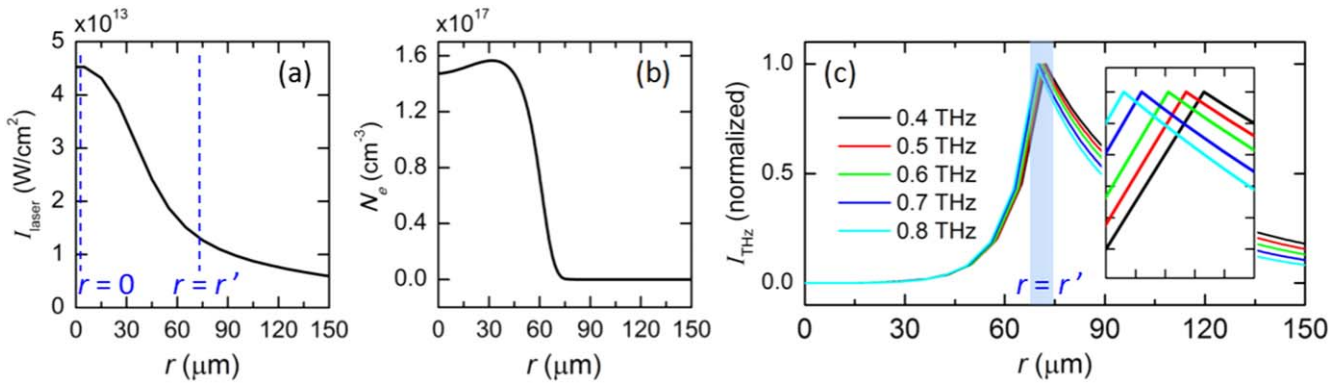

Figure 7. The simulated distributions of I_{laser} (a) and N_e (b) as a function of r. (c) The calculated THz mode field intensity I_{THz} distributions at five frequencies. Inset: enlarged view of the shaded area.

filament, the emitted THz pulse should be in elliptical polarization due to birefringence inside the filament [23]. However, in this work, the final output of THz wave has been detected in linear polarization (figure 4(c)). The effect giving rise to the THz polarization evolution from elliptical to linear during filamentation (figures 4(a)–(c)) is still unknown. Next, we firstly discussed the birefringence effect in detail in section 2.3. Then, in section 2.4, we revisited figure 3 for new clues.

2.3. Laser-induced birefringence effect along the plasma filament

As evidence of the existence of birefringence effect, the generated $E_{\text{THz},x}$ and $E_{\text{THz},y}$, extracted from figure 3 at $z = 1$ and 20 mm, are shown in figures 5(a) and (b), respectively. In view of the relative temporal delay between $E_{\text{THz},x}$ and $E_{\text{THz},y}$, one may firstly think of the reported THz birefringence along the filament [21–23, 40]. Briefly, $E_{\text{THz},x}$ and $E_{\text{THz},y}$ travelled at different velocities in the filament zone, which finally resulted in an elliptically polarized THz radiation. The origin of this birefringence effect can be explained by the difference of pump-induced nonlinear contributions to n_x and n_y along two orthogonal polarization directions [40–43]. For instance, the refractive index modulation caused by the Kerr effect is given by $\Delta n_{x-y} = 4\ n_2\ I_{\text{laser}}/3$ [43], where I_{laser} is the pump laser intensity inside the filament.

Next, the z range has been extended on the basis of figure 3, in which $z = 0$ mm denotes the starting position of the CB measurement, instead of the starting point of the filament. The whole range of z axis is shown in figure 5(c), in which the plasma density (N_e) of the filament is plotted as a function of z. One can see that the filament started at around $z = -20$ mm. We carried out the detection of THz pulses from $z = 0$ mm in order to achieve better signal-to-noise ratio. At $z = 0$ mm, the THz wave might have already experienced birefringence effect for about 20 mm (from $z = -20$ to $z = 0$ mm). According to [23] whose experimental situation is similar with ours, a 2 cm long filament could result in a 100 fs relative delay between $E_{\text{THz},x}$ and $E_{\text{THz},y}$. This value agrees with our data of 115 fs as shown in figure 5(a).

Afterwards, due to the off-axis propagation of THz wave in the high-N_e region of the plasma column (described in detail in section 2.5), the local laser intensity $I_{\text{laser}}(r')$ decreased by more than three times. In this case, the I_{laser}-induced birefringence effect like Δn_{x-y} ($=4n_2\ I_{\text{laser}}/3$) would also approximately decrease by the same order of magnitude. Thus, the newly generated THz pulses from longitudinal positions of the filament in the off-axis propagation range (from $z = 0$ to $z = 20$ mm) would undergo 3-times weaker birefringence. The corresponding retarded time between $E_{\text{THz},x}$ and $E_{\text{THz},y}$ is expected to be around 30 fs ($\approx$100 fs/3). If additionally taking into account of the THz pulses generated before $z = 0$ mm whose retarded time between $E_{\text{THz},x}$ and $E_{\text{THz},y}$ is 115 fs, the overall THz outputs at $z = 20$ mm would have a relative temporal delay larger than 30 fs but smaller than 115 fs. Here, the experimental results are shown in figure 5(b), which are extracted at $z = 20$ mm in figure 3. It can be seen that the relative delay between $E_{\text{THz},x}$ and $E_{\text{THz},y}$ is 51 fs, in agreement with the above prediction.

2.4. Evidences of THz wave propagation inside the filament

Revisiting figure 3, it can be clearly seen that the phenomenon of temporal advance of THz amplitude maxima took place in both orthogonal directions. The dashed lines have highlighted this tendency by marking the peaks of the THz waveforms at each z, and the horizontal solid line is for contrast. As demonstrated in [29, 44], this temporal advance of the THz transient is a good indicator of THz wave propagation inside the plasma column, during which the THz refractive index is below the unity and thus the THz pulse has a superluminal phase velocity.

Another evidence of the THz wave propagation effect could be the THz spectral width variation with respect to the plasma density (N_e) within the filament region. Here, Fourier transformations have been performed on the THz waveforms generated from each longitudinal point of the filament, which are obtained by differentiating the measured THz waves shown in figure 3(a). The Fourier transformed THz spectral amplitudes are shown in figures 6(a) and (b), before and after normalization, respectively. Figure 6(c) further displays the

distribution of THz spectral FWHM along the filament, which is extracted from figure 6(b). For straight comparison, the corresponding $N_e(z)$ distribution (achieved by side-imaging method [45]) has also been indicated in figure 6(c). The anti-correlation between THz spectral width and N_e can be clearly noticed, and the spectral width narrowing mainly occurred in high frequency band (figure 6(b)). These features agree well with the conclusions drawn in [32], which has attributed the spectral width narrowing with the increasing N_e to the THz-plasma interaction during THz wave confined propagation along the plasma channel. For detailed information, please refer to section 2C of [32].

It is worth mentioning that, different from our result, THz bandwidth increases with the increasing ambient gas pressure (or N_e) has been reported in the literature [26, 46–49]. Various theories have been proposed to describe the nature [26, 46–49]. Impressively, in all these publications, ultra-broadband THz spectrum emissions (up to tens of terahertz) were studied, either by simulations [46, 49] or by experiments (with a Michelson interferometer) [26, 47, 48]. Nevertheless in this work, a traditional ZnTe-based EOS detection system with limited detectable bandwidth was employed. The recorded peak frequency was only 0.6 THz and the detected spectral range was from 0.2 to 0.9 THz (figure 6(b)).

This low THz band, however, would make a very different situation from the broad and high THz band studied in the literature [26, 46–49], since THz frequency (f_{THz}) of 0.2–0.9 THz coincides the plasma frequency (f_p) within the filament area. f_p could be calculated by $f_p = \omega_p/2\pi = [e^2 \cdot m_e^{-1} \cdot \varepsilon_0^{-1} \cdot N_e]^{1/2}/2\pi$, where e represents the electric charge, m_e indicates the effective mass of the electron, and ε_0 is the permittivity in the vacuum. Considering a typical filament with peak N_e value of 1×10^{17} cm^{-3} [50], the corresponding f_p is less than or equals 2.84 THz, covering the whole THz band detected in the current work. Thus, the resonance between THz wave and the filament plasma could occur ($f_{\mathrm{THz}} = f_p$) [31], followed by the off-axis propagation of THz wave inside the plasma column (section 2.5), during which the higher-f_{THz} component (towards 0.9 THz as shown in figure 6(b)) became more leaky with the increasing N_e [32]. Hence, the THz bandwidth (FWHM) decreased as displayed in figure 6(c).

Based on the above discussion, the contradiction of the variation trend of THz spectral width with respect to plasma density (or ambient gas pressure) between this work and the aforementioned publications [26, 46–49] might come from the significantly different THz spectral region being investigated. In our case of low THz band (0.2–0.9 THz), the THz-plasma resonance effect ($f_{\mathrm{THz}} = f_p$) played a crucial role. While this interaction might not be remarkably effective in high frequency band (up to tens of terahertz) due to $f_{\mathrm{THz}} \gg f_p$.

Furthermore, in view of figures 3–6, a question is naturally raised: is there a relationship between the propagation effect of THz wave and its polarization evolution? In order to answer this question, the temporal displacement of $E_{\mathrm{THz},x}$ maximum ($\tau_{\max}$) in figure 3(a) has been plotted in figure 4 as blue open circles, together with the distribution of e (bars). One can see that they closely follow the variation trends of each other, which hints that the THz linear polarization is somehow positively correlated to the THz wave propagation inside the filament. For deeper investigation, numerical simulations have been performed in the following section. It can be seen that the observed reduced ellipticity of THz polarization can be qualitatively interpreted by the off-axis propagation of THz wave inside the plasma filament.

2.5. Numerically simulated off-axis THz mode field inside the filament

In this section, the experimental parameters (please see the paragraph before section 2.1) were adopted as the initial parameters of the simulations. By using nonlinear wave equation (equation (10) in [29]), the radial distributions of the laser intensity $I_{\mathrm{laser}}(r)$ and plasma density $N_e(r)$ inside the cross section of the filament have been inferred at the focus, as shown in figures 7(a) and (b), respectively. One can see that the simulated $I_{\mathrm{laser}}(r)$ has a maximum value of about 4.5×10^{13} W cm^{-2} at $r = 0$, where the corresponding on-axis birefringence induced by the laser intensity is also remarkable [43]. Due to this reason, the final THz output after on-axis propagation along the filament is expected to be in elliptical polarization because of the accumulated time delay between $E_{\mathrm{THz},x}$ and $E_{\mathrm{THz},y}$ [21–23].

Nevertheless, when propagating inside the plasma column, the resulted THz mode field could be off-axis and constrained at $r = r'$, departing from the axis ($r = 0$) of the filament. This result can be seen from the radial distributions of THz intensity at 0.4, 0.5, 0.6, 0.7 and 0.8 THz in figure 7(c), calculated based on the $N_e(r)$ data in figure 7(b) and the previously reported 1DND model [31, 32]. This off-axis THz mode (in ring shape) is also known as the result of the spatial confinement of THz wave inside the filament [29, 31, 32, 44, 45], namely, a unique experimental phenomenon that the THz energy is spatially constrained inside a space which is much smaller than the THz wavelength.

In this case, the local $I_{\mathrm{laser}}(r')$ where THz wave was confined (at $r = r'$ in figure 7(a)) was about 1.3×10^{13} W cm^{-2}, more than 3 times smaller than the on-axis $I_{\mathrm{laser}}(r = 0)$. The corresponding THz birefringence $\Delta n_{x-y}(r')$, which is proportional to $I_{\mathrm{laser}}(r')$ [43], will also be more than 3 times smaller than that on the axis of the filament. On the other hand, the filament plasma has an isotropic contribution to the $n_{\mathrm{THz},x}$ and $n_{\mathrm{THz},y}$ [43]. Therefore, the off-axis $\Delta n_{x-y}(r')$ is mainly determined by $I_{\mathrm{laser}}(r')$ and could have a negligible small value. In this situation, it could be expected that the newly generated orthogonal $E_{\mathrm{THz},x}$ and $E_{\mathrm{THz},y}$ will always be basically in phase during off-axis propagation along the filament, thus the synthesis of all THz wave emissions could approach its original linear polarization (induced by either 4WM [23] or longitudinal plasma oscillations [10]). This is actually what one can see in figures 4 and 5(a) and (b).

Summarizing this section and section 2.3, the THz wave with slight elliptical polarization observed at the beginning of the filament was due to the fact that the plasma density was low there (figure 5(c)), and the resulted off-axis THz wave

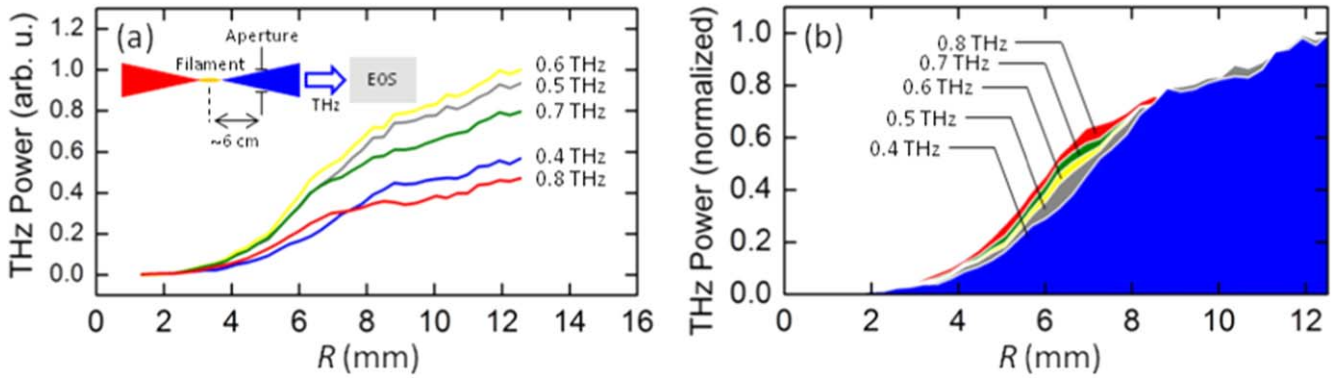

Figure 8. (a) Evolutions of THz power as a function of R at five THz frequencies. Inset: the schematic of profiling the THz beam after the filament. (b) The normalized results of (a).

propagation effect was also weak. Under such circumstances, the THz pulse experienced more (on-axis) birefringence at the beginning of the filament than any other filament region, thus resulting in elliptical polarization (figures 4(a) and 5(a)). Afterwards, the elliptically polarized THz wave gradually evolved into linear polarization (figures 4(c) and 5(b)) by coherence synthesis with qusi-linearly polarized THz pulses newly generated from each longitudinal point of the filament, which acted as a line source with periodic THz emitters.

2.6. Ring-shaped profile of the THz beam in the far field

In order to experimentally verify the aforementioned off-axis propagation of THz wave along the filament column, the emitted THz beam profile has been characterized after the filament in the far field. This indirect demonstration of the THz wave off-axis propagation is the compromise since a more appropriate imaging approach inside the filament is extremely difficult due to the high laser intensity within the filament area.

Here, an aperture was positioned after the filament with a distance of about 6 cm from the middle of the filament, as shown as the inset in figure 8(a). Varying the opening radius R (differed from r in section 2.5) of the aperture, the waveforms of $E_{\mathrm{THz},x}$ were recorded by the EOS setup. Next, by performing Fourier transformations on each THz waveform, the spectral power as a function of R at one certain THz frequency can be retrieved. Figure 8(a) displays such radial distributions of THz spectral power at 0.4, 0.5, 0.6, 0.7 and 0.8 THz. It can be seen that the power distribution at 0.6 THz (yellow line) was the largest since 0.6 THz was the peak frequency of the detected THz spectrum. Moreover, the THz power distribution with respect to R can be divided into three sections: (i) the threshold region ($R < 3$ mm), where THz power was little without much growth; (ii) the rising region (from $R = 3$ to 11 mm), where THz power increased rapidly; and (iii) the saturation region (beyond $R = 11$ mm), where THz power tended to become saturated.

According to the observation of the threshold region in figure 8(a), it can be concluded without any doubt that the THz power distribution pattern on the cross section of the THz beam in the far field cannot be in bell shape. Obviously, a power dip was localized in the beam centre, and the maximum of the THz power lay on an off-axis ring. This feature of THz beam profile is frequently observed in case of two-colour laser pumping due to off-axis phase matching (OAPM) [51]. However, in single-colour case, this ring-shaped spatial distribution of THz power in the far field cannot be interpreted by OAPM [51] which needs both fundamental laser and its second harmonic, or 4WM [23], parametric decay [22], time-varying quadrupoles [18] which three suggest the on-axis directional emission of THz wave.

We remind ourselves that the above THz power ring is in accord with the calculated results shown in figure 7(c). Therefore, the far-field THz power ring may very likely result from the diffraction of the near-field THz ring mode from the end of the filament into the air. In order to clarify this point, the THz power distributions in figure 8(a) have been normalized and shown in figure 8(b). This time, an interesting phenomenon can be observed in section (ii) of R, that the THz power at higher frequency increased faster. This experimental fact hints that the THz power with higher frequency would be located in the inner ring of the far-field THz radiation profile. Once again, this tendency agrees with figure 7(c) (inset) which is demonstrated inside the filament region.

Moreover, if the above aperture test could be performed inside the filament column somehow, the recorded THz power distribution P_{THz} could be foreseen by integrating the simulated $I_{\mathrm{THz}}(r)$ in figure 7(c) with the formula of $P_{\mathrm{THz}} = \int I_{\mathrm{THz}}(r) \cdot 2\pi r \cdot \mathrm{d}r$. The result is shown in figure 9, whose variation tendency is exactly the same with that in figure 8(b).

Hence, the good agreements between the near-field and far-field features of THz power distribution have unfolded the physical picture of the current work: the ring-shaped THz mode field diffracted into air at the end of the filament after off-axis propagation inside the plasma column during which its original linear polarization given by 4WM/longitudinal plasma oscillation was well maintained.

3. Discussion

In the above text, a self-consistent theory associated with 4WM (induced by transverse current (TC)) has been

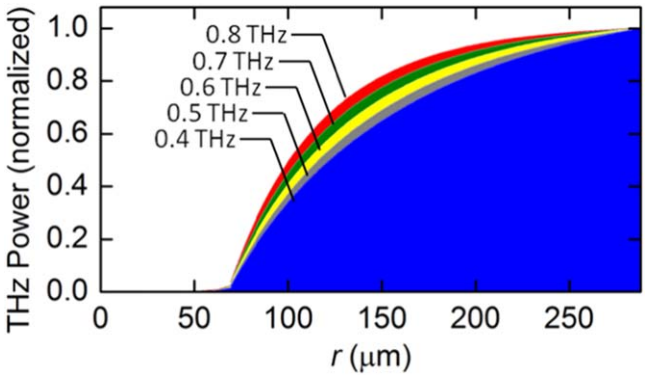

Figure 9. The calculated evolutions of THz power inside the plasma column as a function of r at five THz frequencies.

developed in order to account for the observed evolution of THz polarization state as a function of the filament length. It is worth mentioning that, although non-radial THz polarization (induced by TC) has been studied solely in this work, we do not deny the co-existence of radially polarized THz radiation (induced by longitudinal current (LC)) from a single-colour filament [18, 27]. In fact, it has been proved that both TC and LC contribute to the THz emission during filamentation [19, 27, 52–57], scaling linearly and sub-linearly, respectively, with the increasing ratio between plasma length L_p and THz wavelength λ_{THz} [53]. It can be seen from figure 4(c) in [53] that the ratio of THz power between contributions from TC and LC is about 30 at $L_p/\lambda_{THz} = 40$. So the corresponding THz amplitude ratio of $|E_{THz,TC}|/|E_{THz,LC}|$ (square root of the power ratio) is about 5.5. This reveals the leading role of $E_{THz,TC}$ when L_p is much longer than λ_{THz}. In this case, the generated THz polarization direction should be mainly along that of $E_{THz,TC}$, theoretically.

On the other hand, $L_p/\lambda_{THz} \geqslant 40$ corresponds to $z \geqslant 0$ mm in our experiment if considering the filament started at $z = -20$ mm (figure 5(c)) and the detected λ_{THz} is about 0.5 mm at 0.6 THz (figure 6(b)). Here, the experimental azimuth angle of the THz ellipse is around 40°, with respect to the horizontal direction (x axis), as shown in figures 2 and 4. Nevertheless, no evidence could be found in [52, 53] for establishing a direct connection between such a 40° angle and the $E_{THz,TC}$ polarization direction, in consideration of the horizontally polarized single-colour pump laser used in our experiment.

Furthermore, radially polarized THz pulses given by the LC might not be able to be detected by our present EOS setup. Because the amplitude of the electric field on the top of the THz conical emission is in opposite phase with the bottom one, resulting in a zero signal at the focus located inside the ZnTe crystal [20, 23]. Therefore, a deeper study with an improved detection setup is necessary to clarify whether the observed conical linearly polarized THz beam was superposed by a radially polarized one, or they diffracted in different angles and separated in space, in case of different filament lengths. The L_p-dependent THz polarization output for TC and LC need further verification in order to account for the main observation of this manuscript. This study has the potential to substantially advance the field, which has been planned and is underway.

4. Conclusion

In summary, THz pulse with non-radial (linear) polarization emitted from a single-colour filament has been investigated in this work. The CB measurements have revealed the issue of THz polarization state evolution from elliptical to linear during filamentation. This novel experimental observation, as well as the detected far-field THz radiation pattern, can be well interpreted by two combined effects of 4WM/longitudinal plasma oscillations and off-axis propagation of THz wave inside the filament. This new finding has uncovered the essential role of THz propagation effect when dealing with laser-pumping THz plasma source.

Acknowledgments

This work was supported by Program 213, National Natural Science Foundation of China (11704252, 11574160, 61722111), National Program on Key Basic Research Project of China (973 Program) (2014CB339802, 2014CB339806), the Major National Development Project of Scientific Instrument and Equipment (2017YFF0106300, 2016YFF0100503), the Key Scientific and Technological Project of Science and Technology Commission of Shanghai Municipality (15DZ0500102), Shanghai leading talent (2016–019), and Young Yangtse Rive Scholar (Q2016212).

ORCID iDs

Jiayu Zhao https://orcid.org/0000-0002-7188-8508

References

[1] Redo-Sanchez A and Zhang X C 2008 *IEEE J. Sel. Top. Quantum Electron.* **14** 260–9
[2] Kimmitt M F 2003 *J. Biol. Phys.* **29** 77–85
[3] Hoffmann M C and Fülöp J A 2011 *J. Phys. D: Appl. Phys.* **44** 083001
[4] Tonouchi M 2007 *Nat. Photon.* **1** 97–105
[5] Bratman V L, Litvak A G and Suvorov E V 2011 *Phys.–Usp.* **54** 837–44
[6] Roskos H G, Thomson M D, Kreß M and Löffler A T 2007 *Laser Photonics Rev.* **1** 349–68
[7] D'Amico C, Houard A, Franco M, Prade B, Mysyrowicz A, Couairon A and Tikhonchuk V T 2007 *Phys. Rev. Lett.* **98** 235002
[8] Wang T J, Yuan S, Chen Y, Daigle J F, Marceau C, Théberge F, Châteauneuf M, Dubois J and Chin S L 2010 *Appl. Phys. Lett.* **97** 111108
[9] Hamster H, Sullivan A, Gordon S, White W and Falcone R W 1993 *Phys. Rev. Lett.* **71** 2725
[10] Cheng C C, Wright E M and Moloney J V 2001 *Phys. Rev. Lett.* **87** 213001
[11] Tzortzakis S *et al* 2002 *Opt. Lett.* **27** 1944–6

[12] D'Amico C, Houard A, Franco M, Prade B and Mysyrowicz A 2007 *Opt. Express* **15** 15274–9
[13] Méchain G, Tzortzakis S, Prade B, Franco M, Mysyrowicz A and Leriche B 2003 *Appl. Phys.* B **77** 707–9
[14] Houard A, Liu Y, Prade B, Tikhonchuk V T and Mysyrowicz A 2008 *Phys. Rev. Lett.* **100** 255006
[15] Chen Y, Wang T J, Marceau C, Théberge F, Châteauneuf M, Dubois J, Kosareva O and Chin S L 2009 *Appl. Phys. Lett.* **95** 101101
[16] Manceau J M, Massaouti M and Tzortzakis S 2010 *Opt. Lett.* **35** 2424–6
[17] Buccheri F and Zhang X C 2015 *Optica* **2** 366–9
[18] Jahangiri F, Hashida M, Tokita S, Nagashima T, Hangyo M and Sakabe S 2013 *Appl. Phys. Lett.* **102** 191106
[19] Wu H C, Meyer-ter-Vehn J, Ruhl H and Sheng Z M 2011 *Phys. Rev.* E **83** 036407
[20] Minami Y, Kurihara T, Yamaguchi K, Nakajima M and Suemoto T 2013 *Appl. Phys. Lett.* **102** 151106
[21] Zhang Y, Chen Y, Marceau C, Liu W, Sun Z D, Xu S, Théberge F, Châteauneuf M, Dubois J and Chin S L 2008 *Opt. Express* **16** 15483–8
[22] Jahangiri F, Hashida M, Tokita S, Nagashima T, Ohtani K, Hangyo M and Sakabe S 2012 *Appl. Phys. Express* **5** 026201
[23] Chen Y, Marceau C, Liu W, Sun Z D, Zhang Y, Théberge F, Châteauneuf M, Dubois J and Chin S L 2008 *Appl. Phys. Lett.* **93** 231116
[24] Bai Y, Song L, Xu R, Li C, Liu P, Zeng Z, Zhang Z, Lu H, Li R and Xu Z 2012 *Phys. Rev. Lett.* **108** 255004
[25] Kim K Y, Glownia J H, Taylor A J and Rodriguez G 2007 *Opt. Express* **15** 4577–84
[26] Kim K Y, Taylor A J, Glownia J H and Rodriguez G 2008 *Nat. Photon.* **2** 605
[27] Peng Y, Geng T, Zang X, Chen L and Zhu Y 2016 Completely evolution of Gouy phase shift in longitudinal terahertz wave *41st Int. Conf. on Infrared, Millimeter, and Terahertz Waves (IRMMW-THz)* (IEEE) pp 1–2
[28] Winnerl S, Hubrich R, Mittendorff M, Schneider H and Helm M 2012 *New J. Phys.* **14** 103049
[29] Zhao J, Zhang Y, Wang Z, Chu W, Zeng B, Liu W, Cheng Y and Xu Z 2014 *Laser Phys. Lett.* **11** 095302
[30] Zeng B *et al* 2011 *Phys. Rev.* A **84** 63819
[31] Zhao J *et al* 2016 *ACS Photonics* **3** 2338–43
[32] Zhao J, Liu W, Li S, Lu D, Zhang Y, Peng Y, Zhu Y and Zhuang S 2018 *Photonics Res.* **6** 296–306
[33] Zhang Y, Chen Y, Xu S, Lian H, Wang M, Liu W, Chen S L and Mu G 2009 *Opt. Lett.* **34** 2841–3
[34] Zhao J and Liu W 2015 *J. Electron. Sci. Technol.* **13** 6–13
[35] Xie X, Dai J M and Zhang X C 2006 *Phys. Rev. Lett.* **96** 075005
[36] Kasparian J and Wolf J P 2008 *Opt. Express* **16** 466–93
[37] Couairon A and Mysyrowicz A 2007 *Phys. Rep.* **441** 47–189
[38] Chin S L, Hosseini S A, Liu W, Luo Q, Théberge F, Aközbek N, Becker A, Kandidov V P, Kosareva O G and Schröder H 2005 *Can. J. Phys.* **83** 863–905
[39] Zhao J 2018 Resonant cavity effect of femtosecond laser filament in terahertz band *Laser Phys.* under review
[40] Yuan S, Li M, Feng Y, Li H, Zheng L, Chin S L and Zeng H 2015 *J. Phys. B: At. Mol. Opt. Phys.* **48** 094018
[41] Béjot P, Petit Y, Bonacina L, Kasparian J, Moret M and Wolf J P 2008 *Opt. Express* **16** 7564–70
[42] Calegari F, Vozzi C, Gasilov S, Benedetti E, Sansone G, Nisoli M, De Silvestri S and Stagira S 2008 *Phys. Rev. Lett.* **100** 123006
[43] Marceau C, Ramakrishna S, Génier S, Wang T J, Chen Y, Théberge F, Châteauneuf M, Dubois J, Seideman T and Chin S L 2010 *Opt. Commun.* **283** 2732–6
[44] Zhao J, Zhang X, Li S, Liu C, Chen Y, Peng Y and Zhu Y 2018 *Appl. Phys.* B **124** 45
[45] Zhao J, Chu W, Guo L, Wang Z, Yang J, Liu W, Cheng Y and Xu Z 2014 *Sci. Rep.* **4** 3880
[46] Babushkin I, Kuehn W, Koehler C, Skupin S, Berge L, Reimann K, Woerner M, Herrmann J and Elsaesser T 2010 *Phys. Rev. Lett.* **105** 053903
[47] Kim K Y, Glownia J H, Taylor A J and Rodriguez G 2012 *IEEE J. Quantum Electron.* **48** 797–805
[48] Rodriguez G and Dakovski G L 2010 *Opt. Express* **18** 15130–43
[49] Moradi S, Ganjovi A, Shojaei F and Saeed M 2015 *Phys. Plasmas* **22** 103115
[50] Théberge F, Liu W, Simard P T, Becker A and Chin S L 2006 *Phys. Rev.* E **74** 036406
[51] You Y S, Oh T I and Kim K Y 2012 *Phys. Rev. Lett.* **109** 183902
[52] Thiele I, Nuter R, Bousquet B, Tikhonchuk V, Skupin S, Davoine X, Gremillet L and Bergé L 2016 *Phys. Rev.* E **94** 063202
[53] Thiele I, de Alaiza Martínez P G, Nuter R, Nguyen A, Berge L and Skupin S 2017 *Phys. Rev.* A **96** 053814
[54] Sprangle P, Penano J R, Hafizi B and Kapetanakos C A 2004 *Phys. Rev.* E **69** 066415
[55] Chen M, Pukhov A, Peng X Y and Willi O 2008 *Phys. Rev.* E **78** 046406
[56] Johnson L A, Palastro J P, Antonsen T M and Kim K Y 2013 *Phys. Rev.* A **88** 063804
[57] Kostin V A and Vvedenskii N V 2010 *Opt. Lett.* **35** 247–9